Unusual Phase Behaviour in the Piezoelectric Perovskite System, $Li_xNa_{1-x}NbO_3$

Martin D. Peel, Sharon E. Ashbrook and Philip Lightfoot*

School of Chemistry and EaStCHEM, University of St Andrews, St Andrews, KY16 9ST, UK

*E-mail pl@st-and.ac.uk

Abstract

The system $Li_xNa_{1-x}NbO_3$ has been studied by using a combination of X-ray and neutron powder diffraction and ^{23}Na solid-state NMR spectroscopy. For $x = 0.05$ we confirm a single polar orthorhombic phase. For $0.08 \leq x \leq 0.20$ phase mixtures of this orthorhombic phase, together with a rhombohedral phase, isostructural with the low-temperature ferroelectric polymorph of $NaNbO_3$, are observed. The relative fractions of these two phases are shown to be critically dependent on synthetic conditions: the rhombohedral phase is favoured by higher annealing temperatures and rapid cooling. We also observe that the orthorhombic phase transforms slowly to the rhombohedral phase on standing in air at ambient temperature. For $0.25 \leq x \leq 0.90$ two rhombohedral phases co-exist, one Na-rich and the other Li-rich. In this region the phase behavior is independent of reaction conditions.

Introduction

Although PZT ($Pb(Zr_{1-x}Ti_x)O_3$) remains the industry standard piezoelectric material, there has been enormous effort in the last few years to find a more environmentally benign lead-free replacement.[1] A leading candidate amongst a range of promising materials is the solid solution KNN ($K_xNa_{1-x}NbO_3$).[2,3] Sodium niobate ($NaNbO_3$) itself is an intriguing material, with perhaps one of the most complex temperature-dependent phase diagrams amongst simple perovskites.[4,5,6] Although itself antiferroelectric (orthorhombic, Phase P, space group *Pbcm*) at ambient temperature, $NaNbO_3$ becomes ferroelectric (rhombohedral, Phase N, space group *R*3*c*, Glazer tilt system[7] $a^-a^-a^-$) below 173 K. Depending on sample synthesis conditions, a ferroelectric polymorph, Phase Q (orthorhombic, space group $P2_1ma$, Glazer tilt system $a^-b^+a^-$) can co-exist with Phase P at room temperature.[8,9] Moreover, the orthorhombic ferroelectric phase of $NaNbO_3$ can be made *via* chemical doping; indeed doping as little as 2% of either potassium or lithium, to form the solid solutions $K_xNa_{1-x}NbO_3$ or $Li_xNa_{1-x}NbO_3$, induces both a change in the octahedral tilt system of Phase P and a polarization to produce Phase Q.[10] The composition-dependent phase diagram of KNN has recently been re-analysed and is now fairly well understood,[11,12] but that of LNN has received much less attention. However, several previous studies[13,14,15] point to both interesting electrical properties and also curious phase behavior for the LNN system, which prompts a more thorough re-appraisal of the chemistry and crystallography of this solid solution.

Most of the previous reports on LNN agree that the ferroelectric phase Q is formed at low doping levels ($0.02 < x < 0.14$-0.15). Also, the co-existence of two phases (not fully characterized in previous work) is generally seen for $0.2 < x < 0.95$. However, there is ambiguity over the phase formation at intermediate values of x ($0.1 < x < 0.2$), with some authors reporting the presence of phase Q, and others the presence of a rhombohedral phase, with space group *R*3*c*.[16] A recent publication by Chaker[17] suggested that for values of up to $x = 0.15$, the orthorhombic phase Q was formed exclusively, with a mixture of the orthorhombic and rhombohedral phases formed for $0.2 < x < 0.9$. This is contradicted by a prior publication by Yukyuk *et al.*,[18] in which the presence of phase Q is observed for $0.04 < x < 0.13$, except for a very narrow composition range, around $x = 0.12$, where the rhombohedral phase is curiously suggested to be formed exclusively. Although the

synthetic strategy used in that work is given, no detailed information is provided regarding such parameters as sample cooling rate and the time period between synthesis and analysis. We believe these factors may be relevant as our own preliminary studies of this system suggest that the relative ratios of the phases present in mixed phase (*i.e.*, rhombohedral plus orthorhombic) samples can change, merely as a function of time sitting in air at ambient temperature. In the light of this peculiar behavior, we have carried out a more systematic survey of the LNN system, in which samples are synthesized using a range of annealing temperatures, times and cooling rates, and characterised using X-ray and neutron diffraction and solid-state NMR spectroscopy, enabling us to probe both local and long-range order. We find that annealing temperature and cooling rate heavily influence the nature of the phases formed and their respective ratios. Most strikingly, we find that the analysis of the samples immediately after synthesis can yield very different results to that performed after samples have been standing in air at room temperature for some time. We explore the results published by Yuzyuk[18] and others previously, and find that by using a systematic approach to the variation of synthetic conditions, coupled with careful structural analysis using both diffraction and NMR techniques, we can gain a clearer understanding of the complicated phase behavior in this system.

Experimental Section

Synthesis: LNN ceramics were synthesised using a conventional mixed oxide and carbonate solid-state route. Samples of $Li_xNa_{1-x}NbO_3$ were prepared with x = 0.05, 0.08, 0.1, 0.12, 0.15, 0.2, 0.25, 0.3, then at increments of 0.1 to x = 0.90, and a further composition at x = 0.95. Stoichiometric amounts of Na_2CO_3 (99.9%, Sigma), Li_2CO_3 (99.9%, Sigma) and Nb_2O_5 (99.9%, Alfa Aesar) were dried at 100 °C for 48 hours, ground for 30 minutes under acetone, and pressed into pellets of 10 mm diameter and approximately 2 mm thickness. Samples were subsequently heated at temperatures between 850 and 1050 °C for 18 hours, and allowed to cool using two different rates (information provided in the relevant text). Pellets were then re-ground to produce final powders suitable for characterization. Unless otherwise stated, all X-ray diffraction data

are obtained within 1 day of synthesizing a sample, and neutron diffraction data within three days.

Powder X-ray diffraction (PXRD): Powdered samples were loaded into disks of 3 mm depth, and data were obtained using Cu $K_{\alpha 1}$ radiation with a wavelength of 1.5406 Å. Diffraction patterns were obtained using a Panalytical EMPYREAN diffractometer with a 2θ step size of 0.017°. All data were recorded at room temperature with a 1 hour scan time.

Neutron powder diffraction (NPD): Time-of-flight neutron powder diffraction experiments were conducted using the high-resolution powder diffractometer (HRPD) at the ISIS neutron spallation source at the Rutherford-Appleton Laboratories. The polycrystalline samples (~3 g) were mounted in cylindrical vanadium cans. Data were collected at room temperature. Each scan was counted for 20 μAhr incident proton beam (ca. 30 min).

Diffraction Data Analysis: All diffraction data were analyzed by Rietveld refinement using the General Structure Analysis System (GSAS) software package. Parameters refined included background coefficients, lattice parameters, profile coefficients, isotropic atomic displacement parameters, atomic positional coordinates and phase fractions. Specific details of refinement strategies are given in the relevant text and figure captions.

Solid-state NMR: Solid-state ^{23}Na (I = 3/2) NMR spectra were acquired using a Bruker 600 Avance III spectrometer, equipped with a wide-bore 14.1 T magnet, at a Larmor frequency of 158.746 MHz, at room temperature. Powdered samples were packed into conventional 4 mm ZrO_2 rotors, and rotated at a magic-angle spinning (MAS) rate of 12.5 kHz. ^{23}Na chemical shifts were referenced to 1 M $NaCl_{(aq)}$ using a secondary reference of $NaCl_{(s)}$ (δ_{iso} = 7.8 ppm). Conventional ^{23}Na MAS NMR spectra were obtained using single-pulse experiments, with a pulse length of 1.5 μs and a radiofrequency nutation rate of approximately 100 kHz. A recycle interval of 5 s was used. To remove the second-order quadrupolar broadening multiple-quantum (MQ) MAS experiments were used. These were carried out using a z-filtered triple-quantum pulse sequence, with sign discrimination reintroduced using the States approach.[19] High-power (~100 kHz) pulses were used for triple-quantum excitation and conversion, with a final central-transition

selective (~9 kHz) 90° pulse. All spectra are shown after the application of a shearing transformation, such that the isotropic spectrum[20] (free from all second-order quadrupolar broadening) can be obtained from a projection onto the δ_1 axis. The indirect dimension is referenced according to the convention outlined in Ref. 19.

Results and Discussion

Preliminary Analysis: The full composition region of $Li_xNa_{1-x}NbO_3$ studied ($0.05 \leq x \leq 0.95$) can be usefully broken down into two regions, with differing general phase behavior. Firstly, region 1 between $0.05 \leq x \leq 0.20$, in which Phase Q ($P2_1ma$) exists either exclusively (for x = 0.05) or as part of a two-phase mixture with a rhombohedral phase (for x = 0.08 – 0.20). Secondly region 2, between $0.20 \leq x \leq 0.95$, in which this rhombohedral phase plus a second rhombohedral phase co-exist. Within region 2, both rhombohedral phases can be described using the space group *R*3*c*. One of these phases is Na-rich and isostructural with $NaNbO_3$ phase N (referred to herein as Na-*R*3*c)*, whereas the other is Li-rich and adopts a more distorted $LiNbO_3$-like structure, and is referred to as Li-*R*3*c*. We stress that both these phases can be described as perovskite type and display three-dimensional corner-sharing connectivity of the NbO_6 octahedra. In both cases, the degree of distortion is sufficiently high that the perovskite A-site (Na/Li) is best described as six-coordinated rather than 12-coordinated. . The degree of distortion is more pronounced in the Li-*R*3*c* phase owing to the smaller ionic radius of Li^+ than Na^+; indeed, an alternative description of the $LiNbO_3$ structure is a cation-ordered corundum structure[21].

Region 1: $Li_xNa_{1-x}NbO_3$ (x = 0.05 – 0.20): Substituting small amounts (2-5%) of Li^+ for Na^+ in $NaNbO_3$ results in the exclusive formation of the ferroelectric phase Q, with space group $P2_1ma$. This phase, at the end member composition $NaNbO_3$, has been well characterised in previous literature,[22,23] and the transition from phase P to Q will not be discussed in this work. For a nominal composition $Li_{0.05}Na_{0.95}NbO_3$ (referred to as LNN-5) an annealing temperature of 850 °C and time of 18 hours forms phase Q exclusively, as shown in Fig. 1.

For samples of nominal compositions $Li_{0.10}Na_{0.90}NbO_3$, $Li_{0.12}Na_{0.88}NbO_3$ and $Li_{0.15}Na_{0.85}NbO_3$ (referred to as LNN-10, LNN-12 and LNN-15, respectively), phase Q can be formed alongside a second, rhombohedral phase, Na-*R*3*c*, under certain synthetic conditions, as discussed below. The refined A-site occupancies and lattice parameters of Na-*R*3*c* suggest a continuous solid solution is formed, for values of x up to 0.2, *i.e.*, the Na-*R*3*c* phase formed for LNN-10 has 90% Na and 10% Li occupancy on the A-site (see SI), increasing as the reactant stoichiometry increases. However, the relative phase fractions of Q and Na-*R*3*c* show a strong dependence upon three factors: annealing temperature, cooling rate and time standing at room temperature after synthesis. Each of these is discussed in more detail below.

Annealing temperature: Annealing temperatures of 850 – 1050 °C were employed for the synthesis of samples of LNN-10, LNN-12 and LNN-15. (All samples were slow-cooled at a rate of 2 °C min^{-1} unless otherwise stated). It was found that using lower temperatures than 850 °C yielded incomplete reactions, with reflections from impurities and starting materials observed in the diffraction patterns. Using higher annealing temperatures for each of these compositions led to higher proportions of the Na-*R*3*c* phase being formed in each case, and, consequently, less of phase Q. This observation was confirmed using Rietveld refinements of NPD data, with the biggest reduction in the fraction of phase Q occurring between 850 and 950 °C, as shown in Fig. 2. Furthermore, increasing the mole fraction of Li results in more of the Na-*R*3*c* phase being formed, such that LNN-12 contains more of the rhombohedral phase than LNN-10, 'all other things being equal.' Table 1 shows how the fraction of phase Q varies as a function of composition and annealing temperature, where samples were synthesised 1 day prior to NPD data acquisition.

As the annealing temperature increases, the (220), (031) and (113) reflections from phase Q all noticeably decrease in intensity, whilst the (006) and (112) reflections from the Na-*R*3*c* phase increase, as shown in Fig. 2. A similar trend is observed in LNN-15, where increasing the annealing temperature results in a higher relative phase fraction of Na-*R*3*c*,

with the rhombohedral phase being formed exclusively at 950 °C and above. As the fraction of Li increases, the rhombohedral phase is preferentially formed, with $Li_{0.20}Na_{0.80}NbO_3$ (LNN-20) containing only this phase for all annealing temperatures between 850 and 1050 °C. The nominal composition also plays an important role in determining the relative phase fractions, with the fraction of phase Q decreasing from 83 to 0% over the compositional range $0.1 \leq x \leq 0.2$, for samples annealed at 850 °C

Cooling rate: Two different cooling rates were employed as part of the synthetic strategy – slow-cooling (2 °C min^{-1}) and fast-cooling, whereby the samples were removed from the furnace and cooled in air, at an average of approximately 15 °C min^{-1}. The products were monitored by quantitative Rietveld analysis of PXRD data. The different cooling rates led to the observation of different phase fractions for samples of LNN-10, LNN-12 and LNN-15, 'all other things being equal.' It was found that faster cooling rates favoured formation of the Na-*R*3*c* phase and slower rates favoured formation of phase Q. It was determined, however, that for $x < 0.08$ and $x > 0.20$, the cooling rate did not affect the relative phase fractions formed. When $x < 0.08$ phase Q is always formed exclusively and for $x > 0.2$ two rhombohedral phases are always observed. For example, LNN-12 annealed at 850 °C contained 45% phase Q when slow-cooled, but only 30% when cooled at the faster rate. At 950 °C, the phase Q fraction fell from 9 to 3% when increasing the cooling rate. Additionally, LNN-15 synthesised at 850 °C results in 29% phase Q when slow-cooled, but this falls to 5% when cooled at the higher rate. The observation that slow-cooling favours formation of phase Q over Na-*R*3*c* seems counter-intuitive in the light of the observations described in the following section. If the high-temperature region of the phase diagram in this composition region has a complexity comparable to that of $NaNbO_3$ itself[4] it may be that an 'easier' pathway to phase Q rather than Na-*R*3*c* is available on cooling. An *in situ* high-temperature diffraction study across the region$0.08 < x < 0.20$ might be helpful in this regard.

When considering any one composition, the annealing temperature and cooling rate used do not affect the lattice parameters of the Na-*R*3*c* phase significantly, with variations almost within the standard errors associated with Rietveld refinements using the GSAS

software. As an example, the lattice parameters determined for LNN-12 (synthesised using different conditions) are shown in Table 2. For a range of samples, in general there is a very small decrease in the *a*-parameter and a small increase in *c* when greater annealing temperatures are used. By comparing these small changes to the plot of lattice parameters versus x (Fig. 7), it can be deduced that only a very small reduction in Na content would be needed to change the lattice parameters by the observed amount, of the order of less than 1%.This may imply that a small amount of Na is lost due to volatility at higher temperatures.

Time at ambient temperature after synthesis: In the compositional region $0.05 \leq x \leq 0.15$, changes occur in the relative phase fractions after samples are left standing at ambient temperature (in air) over a period of time. It is observed that the relative fraction of phase Q reduces over time for many samples, as discussed below. There are two distinct ways in which these transformations may occur – firstly, phase Q may have degraded to an amorphous phase, or secondly, it could undergo a subtle structural rearrangement to the Na-*R*3*c* phase directly. We have no reason to suppose a change of stoichiometry during these processes. ^{23}Na (14.1 T) MAS NMR experiments showed no evidence for the presence of any Na-containing impurities, including amorphous phases which may be undetectable by diffraction methods. Furthermore, PXRD measurements using an Al_2O_3 standard confirmed that, although the relative phase fractions of Q and Na-*R*3*c* change, the absolute amount of LNN phases remains unchanged, i.e., phase Q undergoes a crystal-to-crystal phase transition directly to the Na-*R*3*c* at room temperature. Recent reports in the literature confirm that similar non-diffuse phase transitions occur in other perovskite materials.[24]

Using Glazer notation, phase Q has the $a^-b^+a^-$ tilt system, and Na-*R*3*c* has the $a^-a^-a^-$ tilt system, as shown in Fig. 3. The conversion from phase Q to Na-*R*3*c* is subtle and only requires a single in-phase tilt to become out-of-phase, with cooperative cation displacements. This conversion is consistent with Phase Q being only metastable with respect to the Na-*R*3*c* phase within this composition range. Interconversion of the Q and Na-*R*3*c* phases are observed for LNN-10, 12 and 15 on timescales varying between a

week and a year, as shown in Fig. 4. For a sample of LNN-10 synthesised at 950 °C, the fraction of phase Q fell from 21% to 11% over a 14 day period, with an intermediate fraction of 18% observed after 7 days. After 14 days, the rate of decrease appeared substantially slower, and approximately equal to 1% per week over a subsequent 4 week period. For LNN-12 samples synthesised at 850 °C a reduction in the fraction of phase Q was also observed with time; from 47% to 35% phase Q over 14 days for a sample which was slow-cooled, and from 30% to 24% over 14 days when the sample was quenched. After this time, the rate of decrease of phase Q was approximately 1% per week for both samples, and difficult to accurately determine owing to the quantitative limitations of the refinement using GSAS. A separate sample of LNN-12 synthesised at 850 °C, however, showed the complete removal of phase Q after 12 months. Initially, PXRD confirmed that there was a 45% fraction of phase Q, yet this was absent completely 1 year later. This latter observation prompted our subsequent investigation of the variation of phase fractions with time, and, consequently, intermediate data points (such as weekly or monthly) are not available. A sample of LNN-15 synthesised at 850 °C initially with 45% phase Q, showed complete absence of this phase after 12 months (again no intermediate data points are available). The changes in these fractions and their corresponding rates, can also be observed using ^{23}Na MQMAS NMR spectroscopy. MQMAS NMR experiments are an excellent probe of local structure and disorder, and ^{23}Na MQMAS spectra have provided detailed structural information in similar $NaNbO_3$ phases.[25] MQMAS experiments are required to resolve the distinct Na sites (2 for phase Q and 1 for Na-*R*3*c*, as shown in Fig. 5 with values listed in Table 3), and the variation of the different phase fractions can be monitored using the isotropic projections of the spectra. Examples of the variation over time in the isotropic spectra are shown for LNN-10 and LNN-12 in Fig. 6. It should be noted that when determining which resonances correspond to each phase in the mixed-phase samples, the magnitude of P_Q, the quadrupolar product, is a good indicator. Typically, the isotropic shifts may be used, but owing to the different amounts of Li and Na in the samples, these change as the local environment varies, as shown in Table 3. Additionally, the resonances corresponding to Phase Q show increased peak broadening for LNN-10 than for LNN-12 (Fig. 5), owing to the increased disorder as the lithium fraction increases over this region.

The slow reaction kinetics relating to this ambient temperature transformation of phase Q to Na-*R*3*c* may be related to the very similar thermodynamic stabilities of the two phases: our recent DFT studies[4] on pure $NaNbO_3$ show that the energetic stabilities of the various polymorphs observed versus temperature differ by only very small amounts, in particular phase Q and phase N differ by around 0.006 eV per formula unit (~ 0.6 kJ mol^{-1}). There may also be a kinetic barrier caused by strain effects in transforming from phase Q to Na-*R*3*c* .

Region 2: $Li_xNa_{1-x}NbO_3$ (x = 0.25 – 0.90): In this compositional region, two rhombohedral phases are formed: one Na-rich (Na-*R*3*c*) and the other Li-rich (Li-*R*3*c*). Preliminary PXRD measurements showed that the relative phase fractions appear independent of annealing temperature, cooling rate and time left at ambient temperature, suggesting the phases have fixed compositions and similar stabilities. For both phases, the greatest crystallinity was achieved when using the higher annealing temperature of 1050 °C, and this was used in all syntheses of samples in this compositional range. Further, quantitative structural analysis was carried out using NPD. The lattice parameters of the Na-*R*3*c* phase (shown in Fig. 7) show an interesting trend over the entire LNN series, which is supported by systematic variations in Nb and Na displacements versus composition, as discussed below. The plot of lattice parameters as a function of composition shows two distinct regions: $0.10 \leq x \leq 0.30$ and $0.30 \leq x \leq 0.90$, for which the former shows a linear change with x, and the latter a negligible change in lattice parameters as the reactant composition varies. This is suggestive of a region ($0.10 \leq x \leq 0.30$) where a solid-solution is formed as Li substitutes into phase Na-*R*3*c*: this phase co-exists with a second phase, either Phase Q at low x, or Li-*R*3*c* at higher x. In this compositional range, the refined fraction of Li in the Na-*R*3*c* phase increases monotonically as the stoichiometric amount of Li used in the synthesis increases and the lattice parameters change accordingly, *i.e.*, Vegard's law is observed. As might therefore be expected, the change in lattice parameters for this phase correlates well with the Na:Li ratio. Table 4 gives the relative ratios of Na and Li in both rhombohedral phases for LNN samples with $0.3 \leq x \leq 0.9$. The composition of both rhombohedral phases does not

appear to change significantly when x > 0.30, indicating a miscibility gap between the most stable Na-*R*3*c* and Li-*R*3*c* compositions. To compensate for the overall change in reactant stoichiometry, the relative fractions of these two phases present changes linearly as x increases, as shown in Fig. 8, with more of the $LiNbO_3$-like phase formed when the Li content is higher. By extrapolating the phase fractions (from Fig. 8), an estimate of the limiting compositions of the two phases can be made as $Li_{0.22}Na_{0.78}NbO_3$ and $Li_{0.96}Na_{0.04}NbO_3$, respectively. These compositions are in very good agreement with those determined directly by Rietveld refinement of the site occupancies within the two phases in the miscibility region, as shown in Table 4.

When x = 0.96 only the Li-*R*3*c* phase remains, which is isostructural with $LiNbO_3$. The refined NPD Rietveld profile for LNN-96 can be found in the SI, along with corresponding structural parameters for this phase and for pure $LiNbO_3$ for comparison. Slight differences between the two structures are compatible with a limited solid-solubility range ($0.96 < x < 1.00$) for the Li-R3c phase.

Changes in Na(Li)-O and Nb-O bond lengths, within the composition range $0.1 < x < 0.9$) can also be divided into two distinct regions (Fig. 9). In the Na-*R*3*c* phase each cation site is octahedrally coordinated, with three 'long' and three 'short' bond lengths. For the solid-solution region ($0.10 < x \leq 0.30$) a linear change in bond length with composition is observed, with both the Na(Li)-O and Nb-O octahedra becoming more distorted as x increases. This effect is most appreciable when considering changes in the shorter Na(Li)-O bond lengths. Changes in bond lengths for samples with x > 0.30 are, however, much less pronounced, with the Na(Li)-O bond lengths (Figs. 9c and d) being much more consistent over this range, but the Nb-O bonds (Figs. 9a and b) still showing a small variation. This suggests that the NbO_6 octahedra do not distort significantly, but instead that the Nb cations displace to an off-centre position. The continuing change in the Nb-O bond lengths within a region of apparently fixed composition (x > 0.3) may be an artifact due to approximations in the refinement models used, or may be a genuine effect due to some slight off-stoichiometry or anti-site defects (*e.g.*, a small incorporation of Li on the Nb site, as seen in melt-grown $LiNbO_3$ itself[26]). However, we are unable to

see any meaningful scattering differences in our refinements to account for this. For the Li-*R*3*c* phase, the Nb-O bond lengths are shown in Fig. 9 (e and f). This plot shows two distinct regions, with the region where $0.25 \leq x \leq 0.4$ showing the greatest degree of change, perhaps due to the lower phase fraction and larger error bars. However, beyond this region, there are no noticeable changes in bond lengths and the structure becomes comparable to that of $LiNbO_3$ itself.

The underlying reasons for the extensive miscibility gap in the region $0.25 < x < 0.9$ have not been established, though it is likely that the difference in ionic size and coordination preferences of Na^+ and Li^+ (ionic radii 1.02 and 0.76 Å, respectively in six-coordination) play a part. If the two rhombohedral phases are regarded in the conventional 'perovskite' manner as having 12-coordinate A-sites, the relevant A-O bond lengths are 3 x 2.32 Å, 3 x 2.56 Å, 3 x 3.06 Å and 3 x 3.14 Å for Na-*R*3*c* and 3 x 2.08 Å, 3 x 2.26 Å, 3 x 3.29 Å and 3 x 3.45 Å for Li-*R*3*c*, which demonstrates the incompatibility of the two preferred A-site distortions.

For the Na-*R*3*c* phase when $x > 0.7$ and above, however, ^{23}Na MQMAS spectra reveal the presence of a second Na site (not present in the spectra shown in Fig. 5), as shown in Fig. 10 for LNN-80 (Na1: $\delta_{iso} = -0.8$ ppm and $P_Q = 1.4$ MHz; Na2: $\delta_{iso} = -4.5$ ppm and $P_Q = 0.8$ MHz, see figure for labels). No noticeable changes are observed in the NPD or PXRD data to correlate with this observation, but it is possible that the symmetry is lowered, at least locally, to provide two distinct A-sites, with some tendency towards partial Li/Na ordering. For example, the *R*3 space group, derived simply by removal of the *c*-glide, would contain two crystallographically-distinct Na/Li sites, which may explain the results obtained from ^{23}Na MQMAS NMR. However, as this possible lowering of symmetry occurs only where $x > 0.7$, the fraction of the Na-*R*3*c* phase is relatively low, and no noticeable differences are observed in the Rietveld refinements. Preliminary density functional theory (DFT) calculations and simulations of NMR spectra confirm this phase would show two distinct resonances with different isotropic shifts and quadrupolar products. However, calculations for this phase cannot account for the disorder present (*i.e.*, the inclusion of a small amount of Li), and so cannot accurately

determine the expected isotropic shifts and quadrupolar products, but do provide an estimate for them. The purpose of these calculations was not to accurately determine the ^{23}Na NMR parameters but to confirm that two distinct resonances would be observed in the NMR spectra. Further DFT calculations offer an intriguing possibility for the future but are, at present, beyond the scope of this work.

Conclusions

In summary, we have presented a detailed analysis of the LNN perovskite series $Li_xNa_{1-x}NbO_3$ using complementary diffraction and solid-state NMR techniques. We have synthesised samples using a range of synthetic conditions, all of which have been shown to influence the relative phase fractions observed in the products. Samples of LNN-5 were shown to produce the polar orthorhombic Phase Q exclusively. By manipulating the synthetic conditions employed in making LNN-8, 10, 12 and 15, we are also able to alter the phase fractions of the Q and Na-*R*3*c* phases formed. The Na-*R*3*c* phase is formed preferentially for higher values of x, higher annealing temperature and faster cooling rates. Beyond this region of phase co-existence, *i.e.*, $0.2 < x < 0.9$, two different *R*3*c* phases are formed, one of which (Na-*R*3*c*) is Na-rich and isostructural with phase N of $NaNbO_3$ and the other (Li-*R*3*c*) is Li-rich with a $LiNbO_3$-like structure. Both structures may be regarded as highly distorted perovskites. The composition (22% Li and 96% Li for Na-*R*3*c* and Li-*R*3*c*, respectively) and structure of these two phases appears to be independent of the amount of Li used in the synthesis (for this compositional region only), and annealing temperature and cooling rate have no effect on the nature or proportion of the phases formed. A summary of our findings is presented in Fig. 11.

The time that a sample is left at ambient temperature after synthesis has also been shown to play an important role in determining the relative phase fractions observed for $0.08 < x < 0.15$. The work by Yuzyuk *et al.*[18] confirms the presence of the two phases in this region yet gives very little information about the synthetic conditions used. We have shown that these conditions are very important in determining the phases formed, as well as time between sample synthesis and data acquisition. A thorough systematic study in which these synthetic variables are investigated further is needed to fully understand the

complex LNN system in this composition region. We have shown, through analysis of both diffraction and NMR data, that the fraction of phase Q reduces over time, on a scale of weeks to a year, and consequently, the amount of the *R*3*c* phase increases. We believe this change occurs as phase Q undergoes a subtle structural rearrangement to the more thermodynamically-stable *R*3*c* phase. This conversion requires only one in-phase NbO_6 octahedral tilt to become out-of-phase, with corresponding minor cation displacements. If LNN-based solid solutions are to be considered further for piezoelectric or other properties the observations presented herein need to be borne in mind, and further study is necessary of the details of the structural changes, the behaviour of samples as a function of time and of the corresponding effects on electrical properties. The need for caution when interpreting data published previously is also emphasised, especially where detailed experimental and synthetic strategies are not provided.

Acknowledgements

We thank STFC for provision of neutron diffraction facilities at ISIS and Dr Aziz Daoud-Aladine for experimental assistance. MDP was supported by an EPSRC DTA studentship. NMR facilities were supported by EPSRC under grants EP/J501542 and EP/E041825.

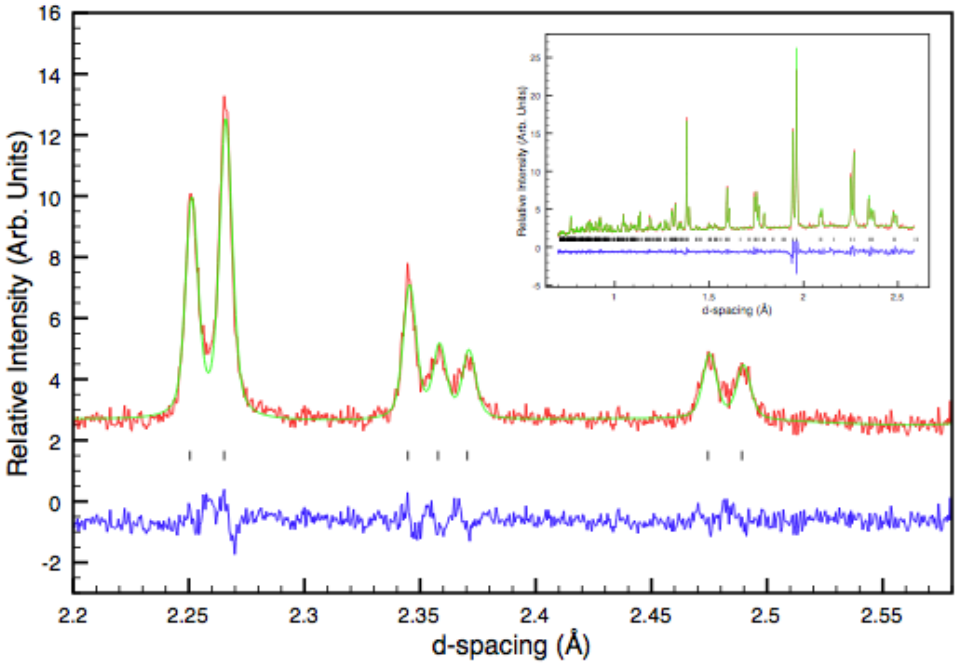

Fig. 1: Portion of the Rietveld refinement (NPD) of LNN-5 highlighting the presence of Phase Q ($P2_1ma$) only. The inset shows the full profile. The red line is the observed diffraction pattern, green is calculated and blue is the difference plot – these standard colors will be used in all subsequent refinement plots. The corresponding crystallographic data table can be found in the SI.

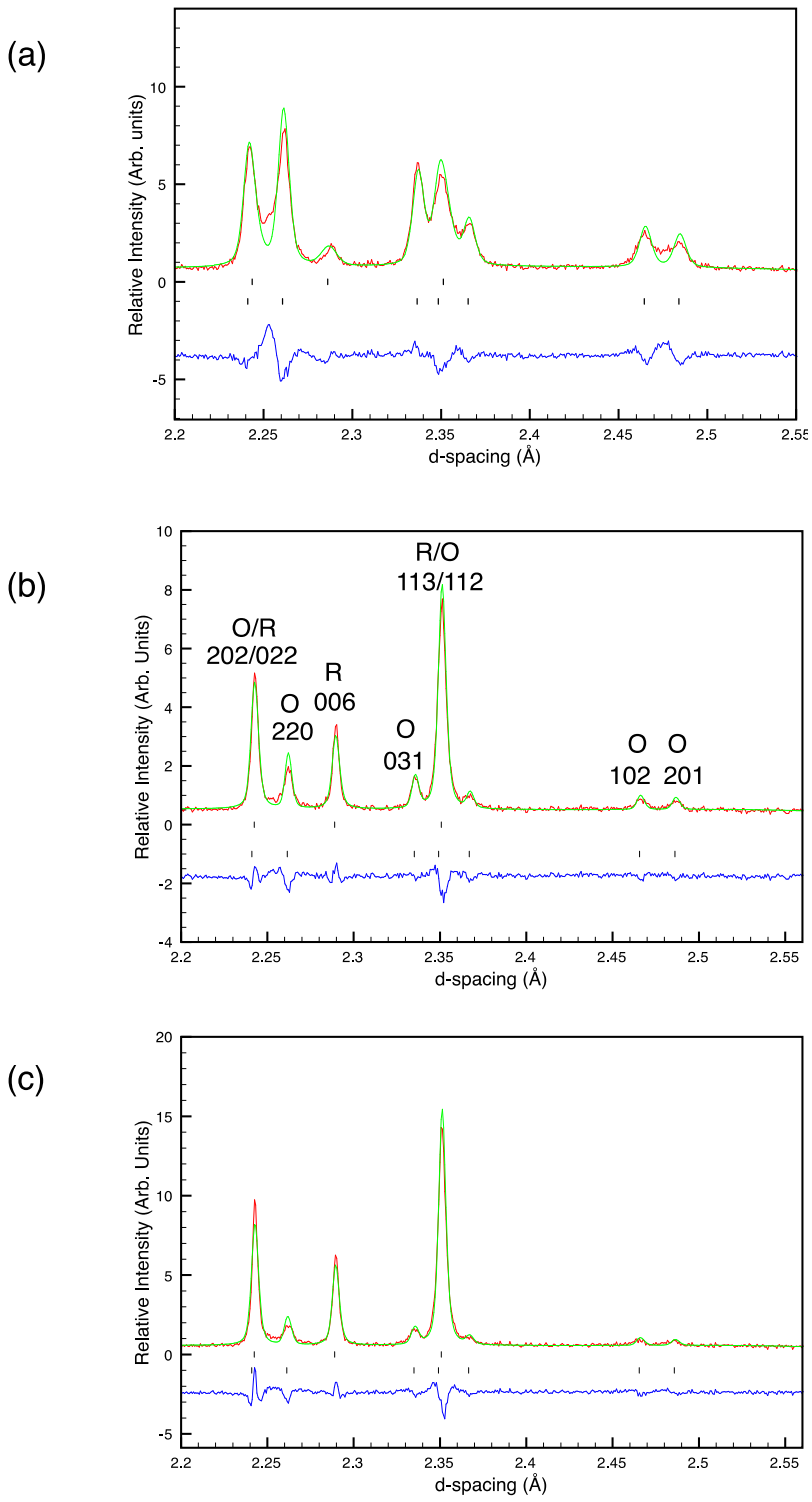

Fig. 2: Portions of the Rietveld refinements (NPD) of LNN-10 synthesised at (a) 850 °C, (b) 950 °C and (c) 1050 °C. Upper-level tick marks represent the Na-*R*3*c* reflections and lower Phase Q reflections, and all major reflections are indexed in the centre pattern only

for clarity: O refers to the orthorhombic Phase Q, R refers to the rhombohedral Na-*R*3*c* phase. In (a), a small peak/broadening present at 2.25 Å is unaccounted for in the refinement; this is not present in (b) and (c) where higher annealing temperatures were used.

Table 1: Fractions of phase Q (NPD data) for three different compositions of LNN annealed at three different temperatures. Note, the values quoted are rounded to the nearest whole number, rather than using the much smaller error derived from Rietveld

Temperature (°C)	**LNN-10 (% Q)**	**LNN-12 (% Q)**	**LNN-15 (% Q)**
850	86	47	31
950	31	6	0
1050	19	2	0

Table 2: Typical lattice parameters of phase Na-*R*3*c* for LNN-12 synthesised using different conditions, obtained from Rietveld analysis of PXRD data.

	Slow-cooled		**Fast-cooled**	
Temperature (°C)	***a* (Å)**	***c* (Å)**	***a* (Å)**	***c* (Å)**
850	5.47461 (6)	13.7338 (2)	5.47452 (6)	13.7337 (2)
950	5.47424 (3)	13.73594(12)	5.47430 (3)	13.73540 (12)
1050	5.47410 (3)	13.73650 (11)	5.47421 (3)	13.73632 (12)

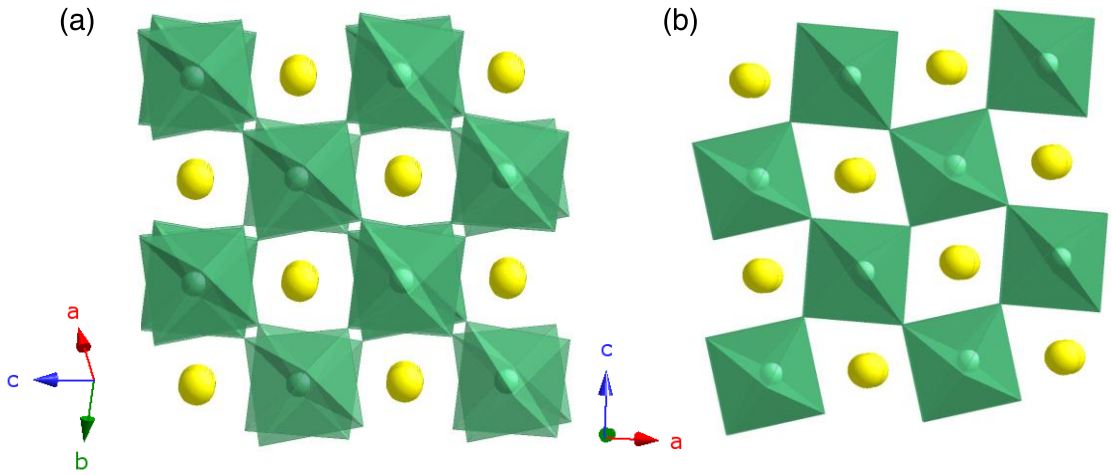

Fig. 3: Octahedral tilting in (a) Phase Na-*R*3*c* and (b) Phase Q, where green octahedra represent NbO_6 units, green spheres are Nb^{5+} cations and yellow spheres are Na^{+}. The required change in tilt mode to convert Q to Na-*R*3*c* can be seen to be subtle. In both phases, each cation site also shows an off-centre displacement.

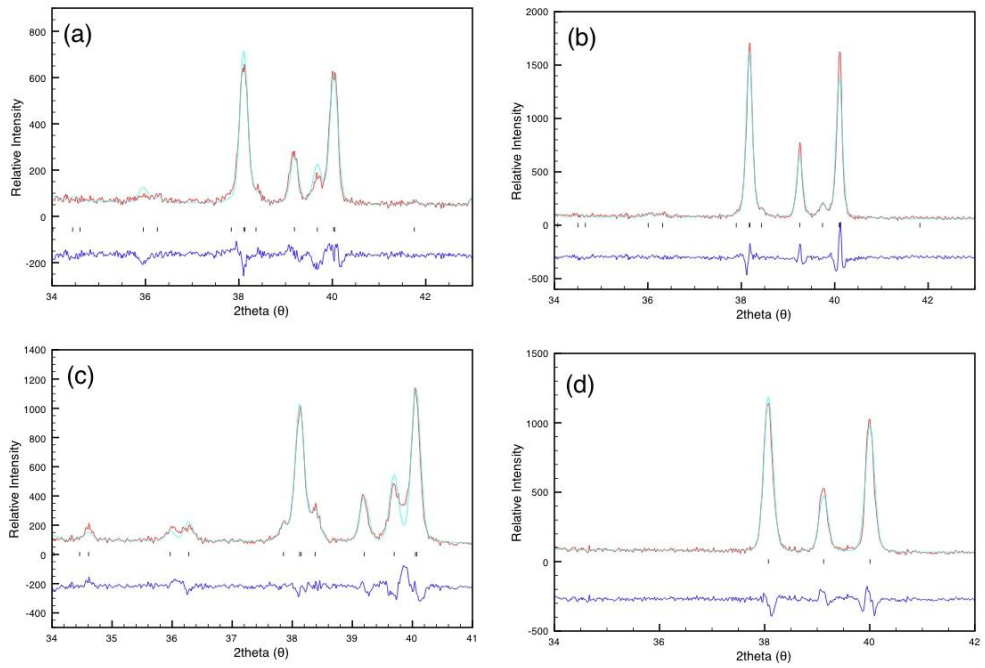

Fig 4: Portions of the Rietveld refinements (PXRD) of (a) LNN-10, 1 day after synthesis (950 °C, 21% phase Q) and (b) 14 days later (11% phase Q), (c) LNN-12, 1 day after synthesis (850 °C, 45% phase Q) and (d) 12 months later (0% phase Q).

Table 3: Average ^{23}Na NMR parameters for Phases Q and Na-*R*3*c*, extracted from the MQMAS NMR spectra in Fig. 5. The quadrupolar product, P_Q, is given, as the C_Q could not easily be determined owing to broadening of the resonances from disorder. Sites Na1 and Na2 present in phase Q are labeled in Fig. 5.

Sample	Site	$\langle\delta_{iso}\rangle$ (ppm)	$\langle P_Q \rangle$ (MHz)
LNN-3	Q-Na1	–4.6 (5)	1.1 (1)
	Q-Na2	–0.6 (5)	2.3 (1)
LNN-15	Na-*R*3*c*-1	–0.8 (5)	1.6 (1)
LNN-10	Q-Na1	–3.7 (5)	1.1 (1)
	Q-Na2	0.1 (5)	2.2 (1)
	Na-*R*3*c*-1	–1.2 (5)	1.5 (1)

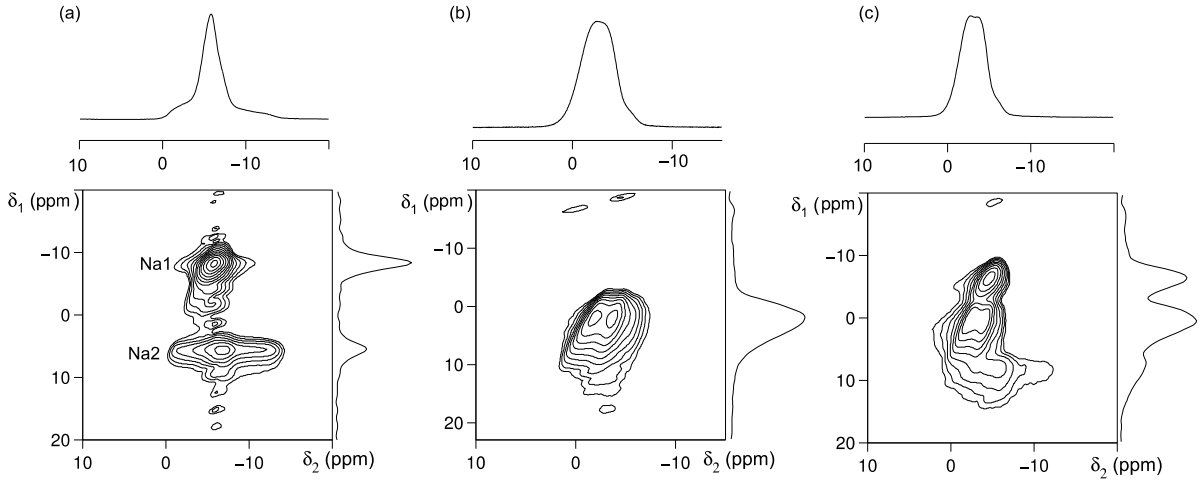

Fig. 5: ^{23}Na (14.1 T) MQMAS and corresponding MAS spectra of (a) LNN-3, Phase Q, (b) LNN-15, Phase Na-*R*3*c* and (c) LNN-10, mixed-phase. The two crystallographically-distinct sites in phase Q are denoted Na1 and Na2. Details of the experiments can be found in the experimental section.

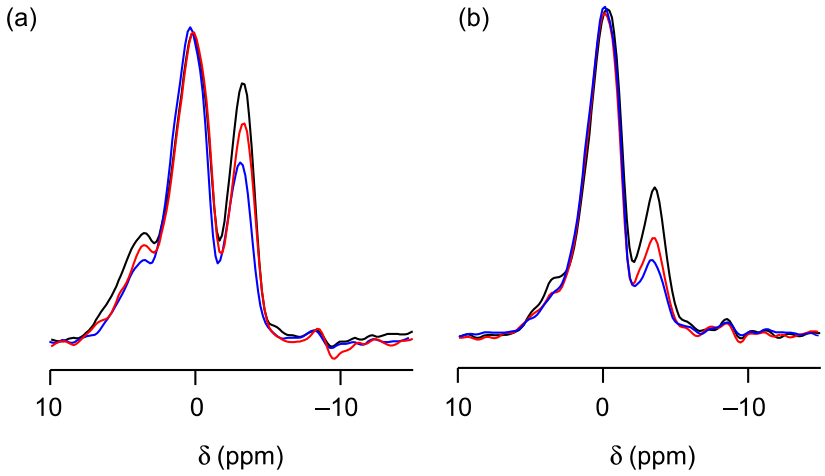

Fig. 6: ^{23}Na (14.1 T) isotropic projections from sheared z-filtered MQMAS NMR experiments for (a) LNN-10 and (b) LNN-12. The lineshapes are scaled relative to the resonance corresponding to the Na-*R*3*c* phase to show the reduction in the Phase Q fraction (the black line is the initial projection, the red and blue lines were obtained one and two weeks later, respectively).

Table 4: Percentage of Na on the A-sites of both rhombohedral phases for samples in region 2, as deduced from Rietveld refinement of NPD data.

Value of x	Na% (Na-*R*3*c*)	Na% (Li-*R*3*c*)
30	77.7 (8)	0.8 (19)
40	79.3 (9)	1.1 (18)
50	78.4 (10)	1.3 (16)
60	78.6 (12)	3.1 (14)
70	80.8 (14)	2.8 (11)
80	79 (2)	3.2 (9)
90	84 (6)	3.4 (9)

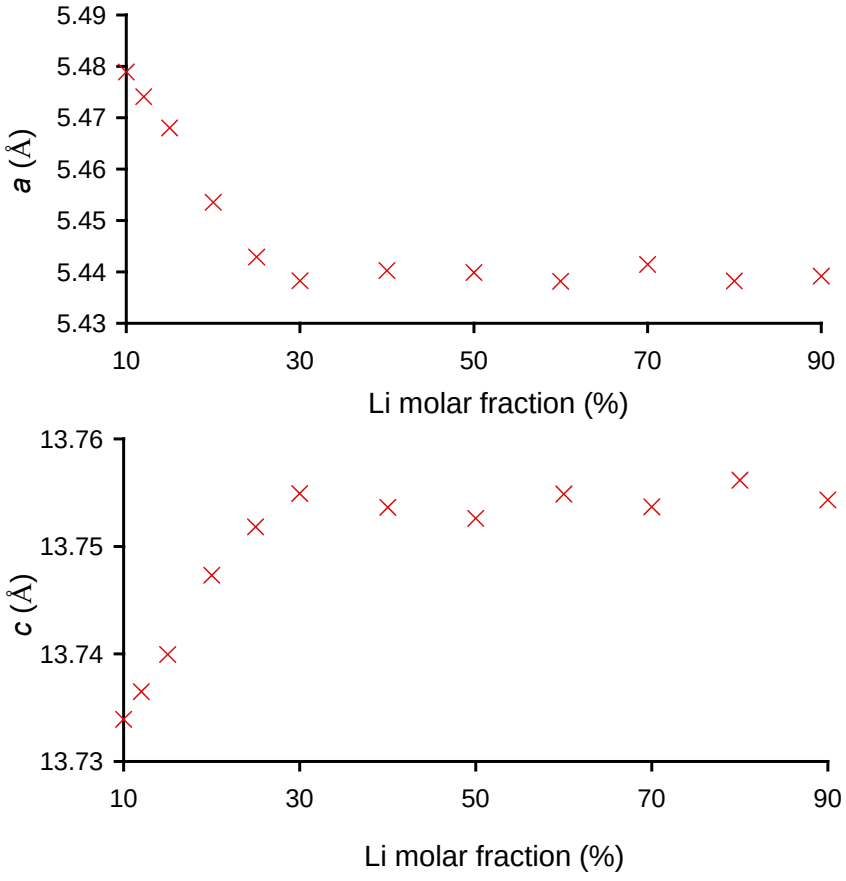

Fig. 7: Lattice parameters for the Na-*R*3*c* phase. Data are obtained from Rietveld refinement of NPD data. Error bars are smaller than the data points and are not shown.

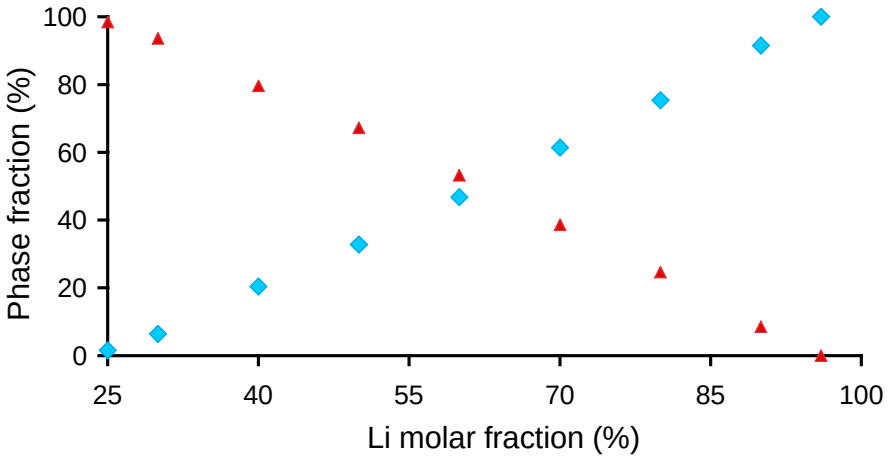

Fig. 8: Phase fractions of the Na-*R*3*c* (red) and Li-*R*3*c* (blue) showing linear variation versus stoichiometry changes.

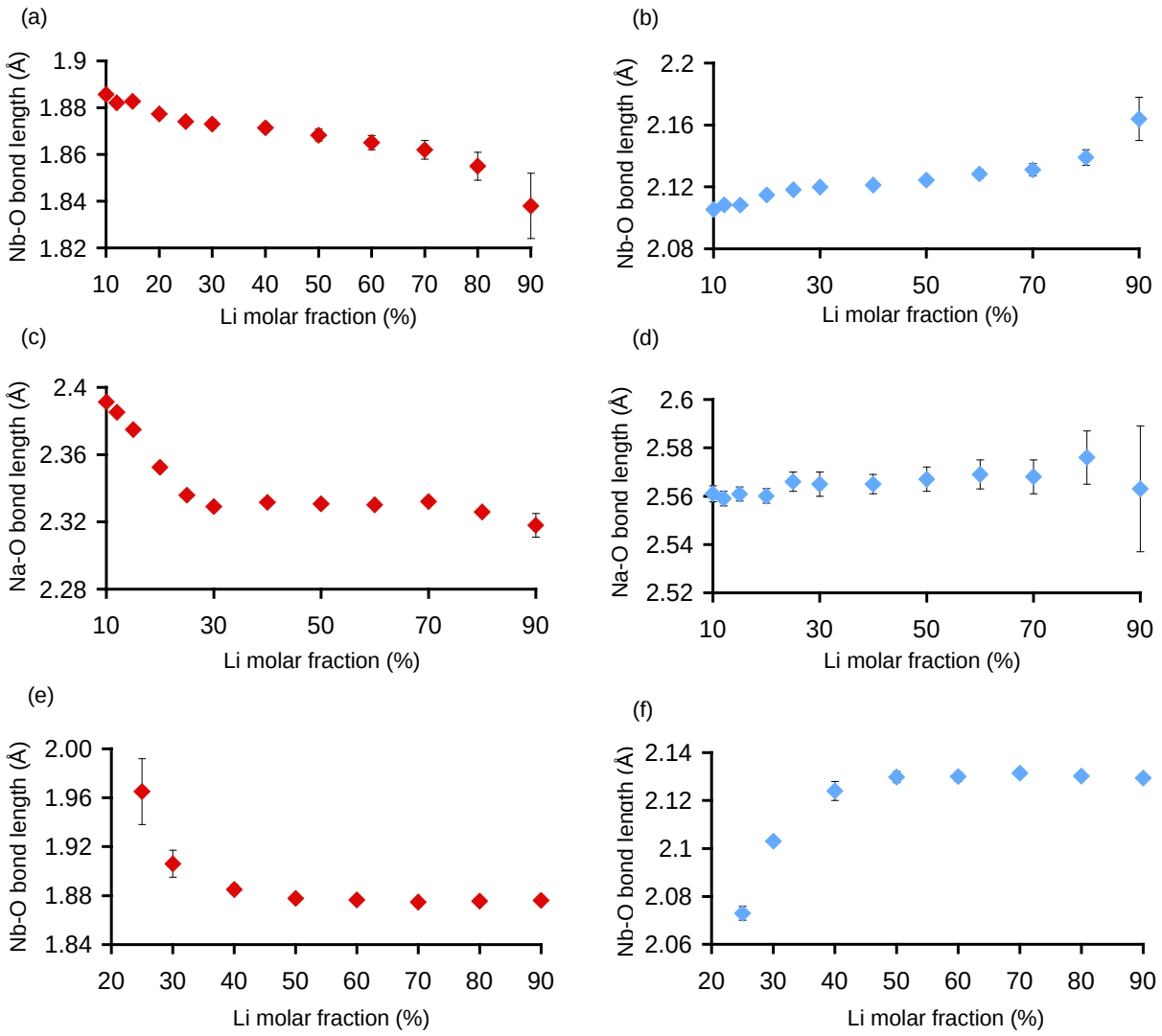

Fig. 9: Nb-O and Li/Na-O bond lengths for the two rhombohedral phases as the reactant stoichiometry (Li molar fraction) is changed. (a) and (b) show the Nb-O bond lengths for the Na-*R*3*c* phase, (c) and (d) show the Na-O bond lengths for the Na-*R*3*c* phase and (e) and (f) show the Nb-O lengths for the Li-*R*3*c* phase.

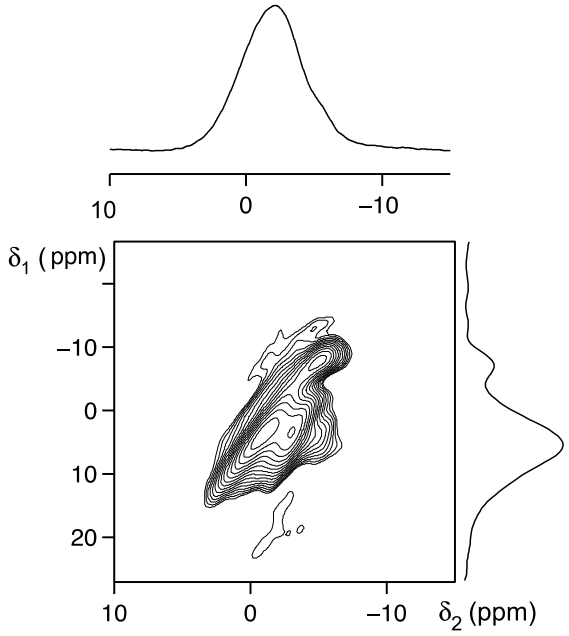

Fig. 10: ^{23}Na (14.1 T) sheared z-filtered MQMAS NMR spectrum of LNN-80, showing two distinct resonances.

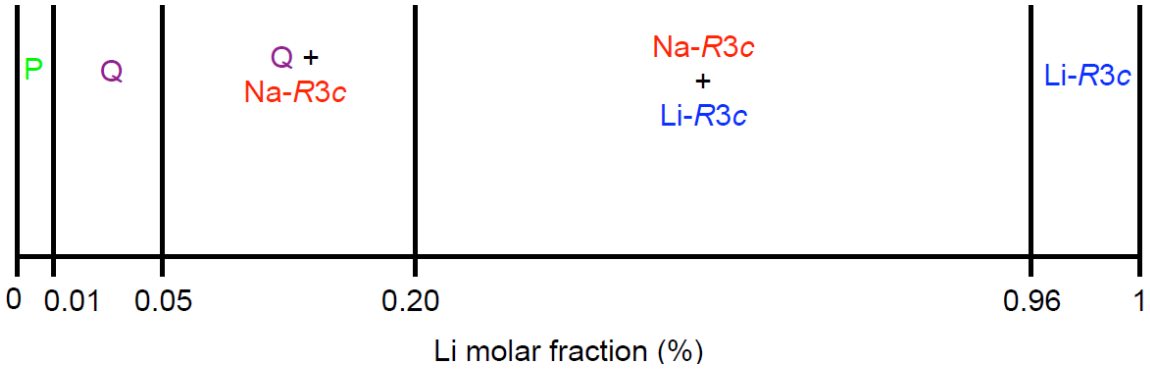

Fig. 11: Schematic compositional phase diagram. P refers to the centrosymmetric phase (space group *Pbcm*).

[1] Cross, E., *Nature,* 2004, **432**, 24.

[2] Saito, Y.; Takao, H.; Tani, T.; Nonoyama, T.; Takatori, K.; Homma, T.; Nagaya, T.; Nakamura, M., *Nature*, 2004, **432**, 84.

[3] Rodel, J.; Jo, W.; Seifert, K. T. S.; Anton, E. M.; Granzow, T.; Damjanovic, D., *J. Am. Ceram. Soc.*, 2009, **92**, 1153.

[4] Peel, M. D.; Thompson, S. P.; Dauod-Aladine, A.; Ashbrook, S. E.; Lightfoot, P., *J. Inorg. Chem.*, 2012, **51**, 6876.

[5] Glazer, A. M.; Megaw, H. D., *Acta Cryst.*, 1973, **A29**, 489.

[6] Glazer, A. M.; Ahtee, M.; Megaw, H. D., *Acta Cryst.*, 1972, **A28**, 179.

[7] Glazer, A. M., *Acta Cryst.*, 1972, **B-28**, 3384.

[8] Johnston, K. E.; Tang, C. C.; Parker, J. E.; Knight, K. S.; Lightfoot, P.; Ashbrook, S. E., *J. Am. Chem. Soc.*, 2010, **132**, 8732.

[9] Shakhovoy, R. A.; Raevskaya, S. I.; Shakhovaya, L. A.; *et al., J. Raman Spec.*, 2012, **43**, 1141.

[10] Ahtee, M.; Glazer, A. M., *Acta Cryst.*, 1976, **A32**, 434.

[11] Zhang, N.; Glazer, A. M.; Baker, D. W.; Thomas, P. A., *Acta Cryst.*, 2009, **B65**, 291.

[12] Baker, D. W.; Thomas, P. A.; Zhang, N.; Glazer, A. M., *Appl. Phys. Lett.*, 2009, **95**, 091903.

[13] Nitta, T., *J. Am. Ceram. Soc.*, 1968, **51**, 623.

[14] Zeyfang, R. R.; Henson, R. M.; Maier, W. J., *J. Appl. Phys.*, 1977, **48**, 3014.

[15] Jimenez, R,; Sanjuan, M. L.; Jimenez, B., *J. Phys. Condens. Matter*, 2004, **16**, 7493.

[16] Mühll, R. V. D.; Sadel, A.; Hagenmuller, P., *J. Solid State Chem.*, 1984, **51**, 176.

[17] Chaker, C.; Gharbi, W. E.; Abdelmoula, N.; Simon, A.; Khemakhem, H.; Maglione, M., *J. Physics and Chemistry of Solids,* 2011, **72**, 1140.

[18] Yukyuk, Y. U.; Gagarina, E.; Simon, P.; Reznitchenko, L. A.; Hennet, L.; Thiadière, D.; *Phys. Rev. B,* 2004, **69**, 144105.

[19] Amoureux, J. P.; , Fernandez, C.; Steuernagel, S., *J. Magn. Reson.,* 1996, **123**, 116.

[20] Pike, K. J.; Malde, R. P.; Ashbrook, S. E.; McManus, J.; Wimperis, S., *Solid State Nucl. Magn. Reson.,* 2000, **16**, 203.

[21] Navrotsky, A., *Chem. Mater*., 1998, **10**, 2787.

[22] Sakowski-Cowley, A. C.; Lukaszewicz, K.; Megaw, H. D. *Acta Cryst*. 1969, **B25**, 851.

[23] Johnston, K. E.; Griffin, J. M.; Walton, R. I.; Dawson, D. M.; Lightfoot, P.; Ashbrook, S. E., *Phys. Chem. Chem. Phys.,* 2011, **13**, 7565.

[24]Troyanchuk, I. O.; Karpinsky, D. V.; Bushinsky, M. V.; Khomchenko, V. A.; Kakazei, G. N.; Araujo, J. P.; Tovar, M.; Sikolenko, V.; Efimov, V.; Kholkin, A. L., *Phys. Rev. B.,* 2011, **83**, 054109.

[25] Ashbrook, S. E.; Le Polles, L.; Gautier, R.; Pickard, C. J.; Walton, R. I., *Phys. Chem. Chem. Phys.,* 2006, **8**, 3423.

[26] Wilkinson, A. P.; Cheetham, A. K.; Jarman, R. H., *J. Appl. Phys.*, 1993, **74**, 3080.